ISSN 2278-3091
Volume 9, No.1.4, 2020
International Journal of Advanced Trends in Computer Science and Engineering
Available Online at http://www.warse.org/IJATCSE/static/pdf/file/ijatcse6691.42020.pdf
https://doi.org/10.30534/ijatcse/2020/6691.42020

L-Band Amplitude Scintillations During Solar Maximum at a Low Latitude Station

Nurliyana Abdul Rahim[1], MohdHezri Mokhtar[1*], NadirulHasraf Mat Nayan[1], Muhammad Yusof Ismail[2], Suhaila M. Buhari[3], Mardina Abdullah[4], Siti Aminah Bahari[4]
[1]Faculty of Engineering Technology, Universiti Tun Hussein Onn Malaysia, 84600 Pagoh, Johor, Malaysia, nurliyanaann@gmail.com, hezri@uthm.edu.my, nadirul@uthm.edu.my
[2]Faculty of Electrical and Electronic Engineering, Universiti Tun Hussein Onn Malaysia, 86400 Parit Raja, Johor, Malaysia, yusofi@uthm.edu.my
[3]Faculty of Science, UniversitiTeknologi Malaysia, 81310 Skudai, Johor, Malaysia, suhailamb@utm.my
[4]Space Science Centre (ANGKASA), Institute of Climate Change, UniversitiKebangsaan Malaysia, 43600 Bangi, Selangor, Malaysia, mardina@ukm.edu.my, sitiaminahbahari@ukm.edu.my
* Corresponding Author: hezri@uthm.edu.my

ABSTRACT

The Global Positioning System (GPS) is one of the most important and useful technologies developed for information and communication technology. Propagated wireless signals along the GPS link are affected by the ionospheric irregularities, therefore the GPS signals may experience ionospheric scintillation. In this study, GPS L-band amplitude scintillations observed at a low latitude station. Data from the Global Navigation Satellite System (GNSS) Ionospheric Scintillation and Total Electron Content (TEC) monitor (GISTM) receiver installed at the Space Science Centre (ANGKASA), Institute of Climate Change, UniversitiKebangsaan Malaysia, UKM (2.92°N, 101.78°E) were used for this study. Of the 460 scintillation (by neglecting S_4<0.15) events recorded during February 2014, 55% were weak (0.15≤S_4<0.25), 32% were moderate (0.25≤S_4<0.35) and 13% were strong (S_4≥0.35). For February 2014, the amplitude scintillations were most pronounced in the post-sunset time to pre-midnight time. Finally, these analysed data are used to study the variability of scintillation with solar activities.

Key words: Amplitude scintillation, GISTM,GNSS, GPS,Low latitude

1. INTRODUCTION

The 24th solar cycle has begun in 2009 and is expected to complete in 2020 when the period of the Sun is least active [1]. The sunspots are the cold dark areas that appear in the solar photosphere [2]. The beginning of the solar cycle is the solar minimum or the least sunspots, while the middle of the solar cycle is the solar maximum with the most sunspots. The solar minimum fades back at the end of the cycle and the new cycle begins. Figure 1 illustrates the solar cycle in which the solar maximum is seen in 2014 and the solar minimum in 2008 and 2020 occurred.

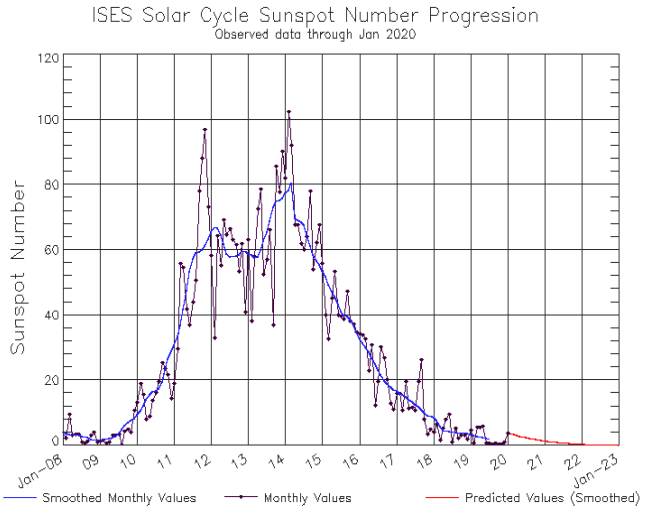

Figure 1: Solar Cycle 24 sunspot number progression (NOAA, 2020)

Figure 2 shows the simulations of the sun where it indicates how movements inside the sun transform the shape and its magnetic field over an 11-year solar cycle. It starts with the solar minimum, the magnetic field of the sun is poloidal, like a bar magnet. Then, the movements in the sun will wind up the fields until they become toroidal. Next, kinks in the fields appear as sunspots, first at mid-latitudes. At solar maximum, sunspots are more common and closer to the equator. While the turbulent motion tears the sunspots apart, the meridional flow shifts the remnants to the poles. The remnants will then cancel the original poloidal field and build up in a new one. At the end of the day, the sun returns to solar minimum, but the polarity of its poloidal field is reversed.

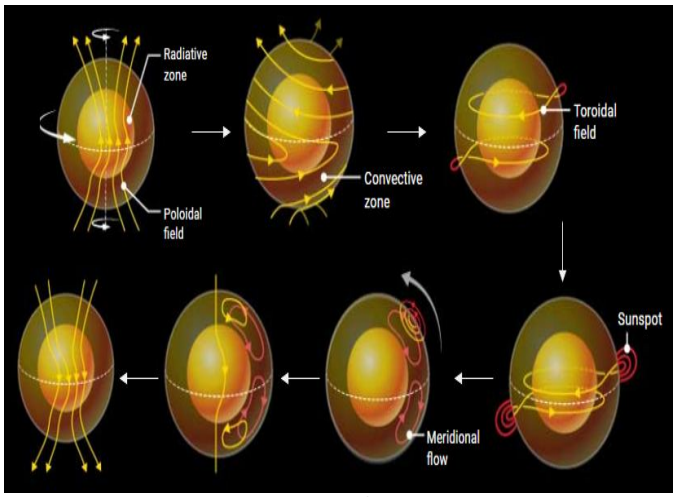

Figure 2:11-year solar cycle transformation (C. Bickel, 2019)

Solar maximum is a regular period of most significant solar activity in the 11 years of the solar cycle of the sun [3]. A large number of sunspots appear and the solar maximum and the sun's irradiance output increases by about 0.07% [3]. Solar activity has a major impact on global scintillation activity, causing scintillation intensity and the incidence of scintillation during peak solar activity is significantly higher than during the minimum solar activity [4]. Scintillation is induced by electron density irregularities that can be categorized by rapid fluctuations in radio frequency signal amplitude and phase and is produced as a signal passes through irregular structures in the ionospheric layer [5], [6].

The ionosphere region divided into three areas, namely: the low latitude regions, middle-latitude regions and the high latitude regions [7]. [8]. Scintillation occurs most frequently in equatorial and high latitude regions and the intense effects are often observed in the equatorial region [6], [9]. Scintillation occurs mainly during local sunset and midnight where usually begins after 18:00 LT, increases in intensity until around 22:00 LT., and slowly decays throughout the night until local early morning hours [5], [6].

A study was conducted to observe scintillation in Guilin from July 2015 to June 2016 and it was found that the amplitude scintillations with $S_4 \geq 0.2$ occurred only in 15 days during this period where all the events took place from 19:00 LT to 05:00 LT on the following day [10]. Observation was made on 5th April 2010 in Malaysia where strong scintillations occurred with $S_4 \geq 0.4$ and the highest value was observed at 19:00 LT to 20:00 LT [11]. Another study in the Indian station Varanasi observed that the scintillation had a maximum percentage of occurrence during the pre-midnight periods [12]. Other than that, a study conducted over Sanya reported weak scintillation but no apparent total electron content (TEC) fluctuation was observed between 12:00 LT to 18:00 LT [13]. It has been shown that scintillation in the equatorial region usually occurs after local sunset and before local sunrise.

The effect of scintillation cannot be neglected and could lead to a significant degradation of the Global Navigation Satellite System (GNSS) which is a system that capable of determining the position of a satellite anytime and anywhere to receive satellite signal as a satellite-based navigation device [14], [15]. One of the GNSS is Global Positioning System (GPS)it is a network of orbiting satellites that transmit back to Earth information of their location in space [16]. The GPS signal is an electromagnetic wave generated by the energy oscillation from the GPS satellite. The GPS signal then propagates along space channel to the GPS user on Earth and this channel is called GPS link. The GPS signal strength decreases due to many factors that affect the quality of the signal depending on the length of the GPS link. This is mainly due to attenuation caused by geometric spreading and the attenuation in the troposphere and ionosphere layers [17].

The GPS has become a powerful instrument for monitoring amplitude scintillation (S_4) and TEC with its multi-satellite advantage, as well as all-weather and all-time monitoring capability. A high sampling rate is needed to obtain scintillation data. Research was conducted using 20 Hz sampling rate to validate the S4 and the rate of change of total electron content (ROTI) [18]. According to the Nyquist Sampling theorem, ROTI derived from observations with higher sampling rates has a better ability to represent ionospheric scintillation because it can monitor small scale irregularities corresponding to the Fresnel scale [19].

The present study intends to focus on Malaysia as it is located in the equatorial region so that the GPS link ionospheric scintillation and availability for this location will be studied and addressed during solar maximum. This paper analyses the scintillation events of February of 2014 as reported by the Australian Government Bureau of Meteorology Space Weather Services, that during the 24th Solar Cycle, the period when the Sun is most active with 146.1 sunspots. Besides, the relationship between amplitude scintillation and ROTI will be established in this paper.

2. INSTRUMENTATION AND DATA COLLECTION

The data used for this study were obtained in February 2014 from Malaysian equatorial GNSS station, the Space Science Centre (ANGKASA), Institute of Climate Change, UniversitiKebangsaan Malaysia, UKM station (2.92°N, 101.78°E), Selangor. The Global Navigation Satellite System (GNSS) Ionospheric Scintillation and Total Electron Content (TEC) monitor (GISTM) receiver experimental set-up consisted of GPS 702 L1/L2 antenna connected with GSV4004B receiver interfaced to a continuous data recording computer (refer Figure 3). The GSV4004B receiver has been specifically designed for ionospheric scintillation measurements on L1 band frequency (1575.42 MHz) and can track up to 11 GPS satellites transmitting for both L1 and L2 band frequencies. It measures amplitude and phase (at the 50-

Hz rate) of the scintillation and the code/carrier divergence (at the 1-Hz rate) for each satellite being tracked on L1 and computes TEC of the combined L1 and L2 pseudorange and carrier phase measurements. Several researchers used this receiver for ionospheric studies [7], [20].

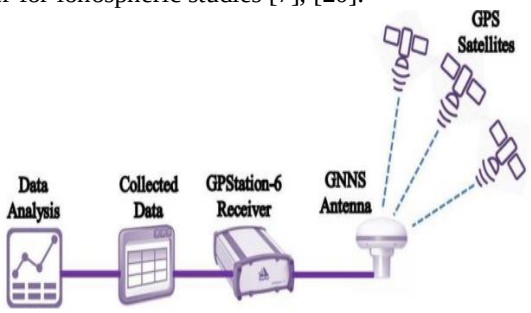

Figure 3: Experimental setup

First, for the climatology part of this study, 30° elevation masking will be used to cut off all non-ionospheric sources (e.g., multipath) from the scintillation data. The percentage of scintillation occurring on the basis of whether or not scintillation has been detected on a daily basis. The monthly percentage of the event was then calculated based on the number of days in the month in which the scintillations were recorded and the total number of days of observations in that month [21].

In this paper, the S_4 index used to study the characteristics of the occurrence of ionospheric scintillations. The raw amplitude scintillation index, S_4, is detrended (by normalization) with the measurements taken at a rate of 50 Hz and then averaged over 60-s intervals [19]. The calculation of the S_4 is performed at 1-min intervals, using signal power, via the following equation:

$$S_4 = \sqrt{{S_{4t}}^2 - {S_{4cor}}^2}$$

where the amplitude scintillation recorded by the receiver has two parameters: total scintillation (S_{4t}) and corrected scintillation (S_{4cor}). The measured S_{4t} recorded by the receiver could be cluttered by the inherent effects of ambient noise and multipath effects [22]. To improve this, the GSV4004B receiver also calculates the correction of the total S_{4t} due to noise and multipath, which is then recorded as S_{4cor}.

During this period, the maximum S_4 recorded (even one value), was used to categorize the strength (weak, moderate, strong) of scintillation as shown in Table 1 [23], [24].

Table 1: Classification criteria for amplitude scintillation

Scintillation Strength	S_4 Scale
Negligible	$S_4 < 0.15$
Weak	$0.15 \leq S_4 < 0.25$
Moderate	$0.25 \leq S_4 < 0.35$
Strong	$S_4 \geq 0.35$

Next, the other scintillation parameter that will be discussed in this paper is phase scintillation, where it is defined as the standard deviation of the carrier phase. Phase scintillation can be calculated as the following equation [25]:

$$\sigma_\varphi = \sqrt{E(\varphi^2) - E(\varphi)^2}$$

Where: σ_φ= Phase scintillation
φ = Carrier phase
E(φ) = Expectation of φ output by GISTM in the interval of 60 s.

The TEC is identified as a measurement of the total number of electrons along a particular path that originates from the satellite and can be presented in the TEC Unit, which is one TECU=electron x 10^{-16}. The TEC itself depends on the activity of the sunspot, seasonal, diurnal and spatial variations and the line of sight that includes knowledge of the satellite's elevation and azimuth [26]. The TEC may be calculated as [18], [22], [27]:

$$TEC = 2(f_1 \cdot f_2)^2 / k\left({f_1}^2 - {f_2}^2\right) \times (L_1 \cdot \lambda_1 - L_2 \cdot \lambda_2)$$

Where: F1 = 1575.42 MHz
F2 = 1227.60 MHz
L1 and L2 = The distance from the satellite to the receiver at f1 and f2
k = 40.3

The rate of change of the total electron content (ROT), calculated from the differential carrier phase, may provide information on large scale electron density irregularities. While the ROT can be deterred as the equation below [22]:

$$ROT = TEC(t + \Delta t) - TEC(t)/\Delta T$$

Where: TEC = Total electron content
Δt = 60 seconds

The TEC fluctuations are commonly characterized by the ROTI parameter, defined as the standard deviation of the ROT rate, calculated for each 1-min or 5-min time interval [20], [22]. It shall be calculated as follows:

$$ROTI = \sqrt{\langle ROT^2 \rangle - \langle ROT \rangle^2}$$

3.RESULTS AND DISCUSSION

The total number of scintillation events for February 2014 is tabulated in Table 2. In the first week of February 2014, 17.2% of the occurrence was recorded and the percentage of occurrence increased to 22.4% in the second week. 26.5% of the occurrence was recorded in the third week and 33.9% was recorded in the final week, which is the highest scintillation week in February.

Table 2: Scintillation events in February 2014

Week	Number of Events	Percentage of Events
1	79	17.2%
2	103	22.4%
3	122	26.5%
4	156	33.9%

Table 3 shows the total scintillation and percentage of occurrence based on the scintillation strength classification. The highest percentage of occurrences recorded at Week 4 (21.8%) followed by Week 3 (17.2%) and Week 2 (2.9%) for strong scintillation. A slight difference can be seen in Week 1 where there was no percentage occurrence recorded for strong scintillation.

Table 3: Total scintillation and percentage of occurrence in February 2014

Week	S_4			Percentage Occurrence		
	Weak	Moderate	Strong	Weak	Moderate	Strong
1	49	30	0	62%	38.0%	0%
2	70	30	3	68%	29.1%	2.9%
3	75	26	21	61.5%	21.3%	17.2%
4	61	61	34	39.1%	39.1%	21.8%

Figure 3 exhibits the overall scintillation occurrence by percentage in February 2014. Figure 4 and Figure 5 illustrates the amplitude and phase scintillation events, respectively. While Figure 6 shows the TEC variation and Figure 7 plotted for all ROTI during the scintillation events. Based on the graphical, all the data were plotted with their corresponding distributions over Universal Time Coordinated (UTC).

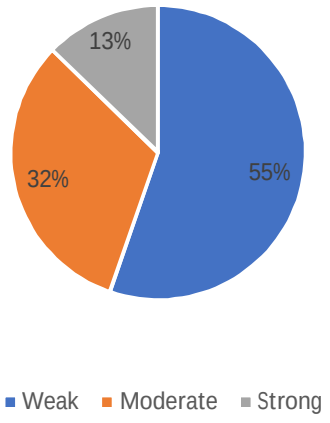

Figure 3: February 2014 percentage occurrence of scintillation

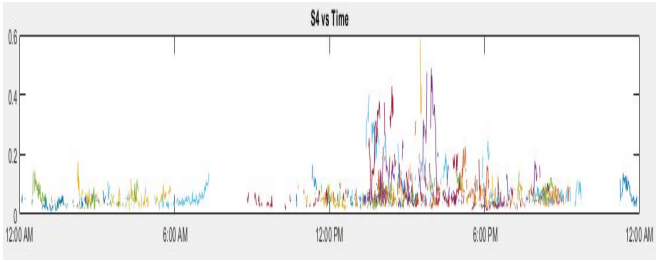

Figure 4: Time series of all S_4 indexes computed each minute (each colour represents one day)

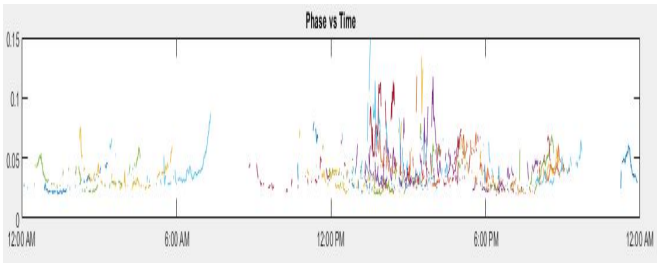

Figure 5: Time series of all phase scintillation indexes computed each minute (each colour represents one day)

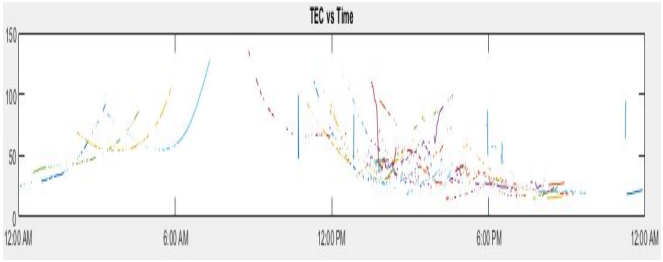

Figure 6: Time variation of all TEC during the scintillation events (each colour represents one day)

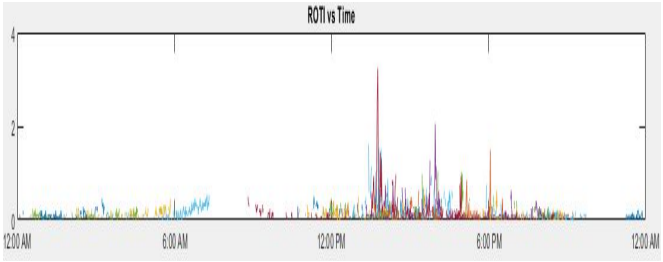

Figure 7: Time variation of all ROTI during the scintillation events (each colour represents one day)

During the solar maximum period; focusing on February 2014, the ionospheric scintillation S_4 index was calculated from the collected data and analysed while considering one GPS satellites for each day. Table 2 presents the number of S_4 events and the percentage of the occurrence. In February, there were 460 scintillations (by neglecting S_4<0.15) of activity. Therefore, by using weekly-basis, we can to demonstrate the percentage of occurrence by their scintillation strength as tabulated in Table 3. The total data in Figure 3 shows that most of the samples recorded had weak amplitude scintillation, some had moderate amplitude scintillation and least had a strong amplitude scintillation.

Referring to Figure 4, the highest amplitude scintillation recorded was less than 0.6. While for the phase scintillation (refer Figure 5) it can be seen that the events recorded will not be more than 0.15 rad. Scintillations over the UKM station were mainly distributed between 13:00 and 18:00 UTC (2100 – 0200 LT) which means after the local sunset and before the local sunrise due to the equatorial irregularities that occurred at post-sunset. Besides, it can be seen that the scintillation activity peaks before local midnight (15:00 UT) and started to vanish around post-midnight (18:00 UT). Based on these results, it has been shown that the equatorial scintillation usually occurs during the post-sunset until the post-midnight hours due to equatorial irregularities which are also known as plasma bubbles occurring in the F-region which can cause scintillation during nighttime [11], [28].

The variation of the TEC was plotted in Figure 6 and shows that the highest TEC recorded around 120 TECU, but some TEC noticed within the hours of 13:00 to 18:00 UTC (2100 – 0200 LT). This is attributed to the fact that the electron density irregularities are usually formed after the local sunset terminator due to ionospheric scintillation. Figure 7 depicted the ROTI values where the highest ROTI value is about 3.2. It can be seen that the ROTI recorded occurred frequently during several scintillation events between 13:00 and 18:00 UTC (2100 – 0200 LT).

During the evening hours in the equatorial region, an enhanced eastward electric field (Prereversal Enhancement is known as PRE, in a zonal electric field) is being developed in the F-region [4]. The rapid loss of molecular ions by recombination after sunset results in a steep vertical plasma gradient at the bottom side of the F-region. Furthermore, this will cause the ionosphere to be unstable due to Rayleigh-Taylor (RT) instability [28]. The relationship between the TEC depletion associated with the plasma bubbles and the corresponding scintillation intensity can be concluded.

4.CONCLUSION

This study elucidates the scintillations of the UKM station during maximum solar activity in February 2014. In the present work focusing on February 2014, out of 460 scintillations (by neglecting S_4<0.15) activities, 256 were weak, 148 were moderate and 59 were strong. Most of the scintillation events occurred during the crucial time between 13:00 and 18:00 UTC (2100 – 0200 LT). However, in the local time post-midnight, the scintillation did not show any apparent variation. Overall, the scintillation appears to have a uniform pattern with the ROTI coefficient. The results of this study may be used for; (i) developing understanding and knowledge on scintillation, specifically in the equatorial region. (ii) further investigation relating with an equatorial plasma bubble phenomenon.

ACKNOWLEDGMENT

The authors thank Universiti Tun Hussein Onn Malaysia for providing funding and full support upon the completion of this paper through GeranPenyelidikanPascasiswazah (GPPS-Vote number H457) and GeranPenyelidikan Tier 1 (Tier 1-Vote number H189). We also thank the Space Science Centre (ANGKASA), Institute of Climate Change, UniversitiKebangsaan Malaysia for the data and knowledge transfer during the visit. We would like to thank the reviewers for their helpful comments and suggestions on this paper.

REFERENCES

1. S. Ismail, T. A. Musa, W. A. W. Aris, and G.Gopir. **Effect of the X5. 4 class solar flare event of solar cycle 24 on the GPS signal reception in Peninsular Malaysia**, *The International Archives of Photogrammetry, Remote Sensing and Spatial Information Sciences*, vol. 42, no. 4, pp. 167-171, 2016.
2. A. Seguí, J. J. Curto, V. de Paula, R. Rodríguez-Gasén, and J. M. Vaquero. **Temporal variation and asymmetry of sunspot and solar plage types from 1930 to 1936**, *Advances in Space Research*, vol. 63, no. 11, pp. 3738-3748, 2019.
3. G.R.T.de Lima, S.Stephany, E.R.de Paula, I.S.Batista, M.A. Abdu,L.F.C.Rezende, M.G.S.Aquino, andA.P.S. Dutra. **Correlation analysis between the occurrence of ionospheric scintillation at the magnetic equator and the southern peak of the equatorial ionization anomaly**, *Space Weather*, vol. 12, no. 6, pp. 406-416, 2014.
4. L. Wang, andY. Zou.**Characteristics of low midlatitude GPS ionospheric scintillations over Australia and Niue**, in *2019 Proc. 6th International Conference on Space Science and Communication*, 2019, pp. 29-34.
5. R. Wang, C. Hu, Y. Li, S. E. Hobbs, W. Tian, X. Dong, and L. Chen. **Joint amplitude-phase compensation for ionospheric scintillation in GEO SAR imaging**, *IEEE Trans. on Geoscience and Remote Sensing*, vol. 55, no. 6, pp. 3454-3465, 2017.
6. Y. Jiao, J. J. Hall, and Y. T. Morton. **Automatic equatorial GPS amplitude scintillation detection using a machine learning algorithm**, *IEEE Trans. on Aerospace and Electronic Systems*, vol. 53, no. 1, pp. 405-418, 2017.
7. W. A. Ahmed, F. Wu, and G. I. Agbaje. **Analysis of GPS ionospheric scintillation during solar maximum at mid-latitude**,in *Proc.IEEE International Geoscience and Remote Sensing Symposium*, 2016, pp. 4151-4154.
8. G. D. O. N. Brassarote, E. M. de Souza, and J. F. G. Monico.**S 4 index: does it only measure ionospheric scintillation?**, *GPS Solutions*, vol. 22, no. 1, pp. 8, 2018.

9. D. Xu, and Y.Morton. **A semi-open loop GNSS carrier tracking algorithm for monitoring strong equatorial scintillation**, *IEEE Trans. on Aerospace and Electronic Systems*, vol. 54, no. 2, pp. 722-738, 2017.
10. S. Wang, and Y. Zou. **A study of multi-frequency GNSS ionospheric scintillations at Guilin, China**, in *Proc.11th International Symposium on Antennas, Propagation and EM Theory*, 2016,pp. 279-282.
11. N. Ya'acob, N.Tajudin, A. L. Yusof, M. Kassim, S. S. Sarnin, and N.Zahraa'Zaharudin.**Investigation of ionospheric scintillation and total electron content during maximum and minimum solar cycle**, in *Proc. 2019 International Symposium on Networks, Computers and Communications*, 2019, pp. 1-6.
12. S. B. Singh, V. S. Rathore, A. K. Singh, and A. K.Singh. **Ionospheric irregularities at low latitude using VHF scintillations during extreme low solar activity period (2008–2010)**, *Acta Geodaetica et Geophysica*, vol. 52, no. 1, pp. 35-51, 2017.
13. B. Ning, G. Li, andK. Liu. **Characteristics of GPS ionospheric scintillation and TEC depletion in the Chinese low latitude region**,in *Proc.2016 URSI Asia-Pacific Radio Science Conference*, 2016, pp. 90-92.
14. G. Sivavaraprasad, R. S. Padmaja, and D. V. Ratnam.**Mitigation of ionospheric scintillation effects on GNSS signals using variational mode decomposition**, *IEEE Geoscience and Remote Sensing Letters*, vol. 14, no. 3,pp. 389-393, 2017.
15. Y. L. Sang. **Business process based GNSS modeling method**,*International Journal of Advanced Trends in Computer Science and Engineering*, vol. 8, no. 6, pp. 2278-3091, 2019.
16. H. R. M. Sapry,A. F. Muzaffar, A. R. Ahmad, S. Baskaran. **The implementation of Global Position System (GPS) among the cement transporters and its impact to business performance**,*International Journal of Advanced Trends in Computer Science and Engineering*, vol. 9, no. 1, pp. 2278-3091, 2020.
17. E. F. Aon, R. Q.Shaddad, A. R. Othman, andY. H. Ho. **Analysis of ionospheric scintillation for global navigation satellite system at UTeM, Malaysia**,in *Proc. 2014 IEEE 10th International Colloquium on Signal Processing and its Applications*, 2014, pp. 37-41.
18. J. O. Olwendo, P. Cilliers, Z. Weimin,O. Ming, and X. Yu. **Validation of ROTI for ionospheric amplitude scintillation measurements in a low-latitude region over Africa**, *Radio Science*, vol. 53, no. 7, pp. 876-887, 2018.
19. W. Wei, W. Li, S. Song, and L. Shao. **Study on the calculation strategies of ionospheric scintillation index ROTI from GPS**,in *Proc. IGARSS 2019-2019 IEEE International Geoscience and Remote Sensing Symposium*, 2019, pp. 9894-9897.
20. T. L. Tran, H. M. Le, C. Amory-Mazaudier, and R. Fleury. **Climatology of ionospheric scintillation over the Vietnam low-latitude region for the period 2006–2014**, *Advances in Space Research*, vol. 60, no. 8,pp. 1657-1669, 2017.
21. A. Seif, M. Abdullah, A. H.Hasbi, and Y. Zou. **Investigation of ionospheric scintillation at UKM station, Malaysia during low solar activity**, *Acta Astronautica*, vol. 81, no. 1, pp. 92-101, 2012.
22. M. H. Mokhtar, N. A. Rahim, M. Y. Ismail, and S. M. Buhari. **Ionospheric Perturbation: A review of equatorial plasma bubble in the ionosphere**,in*Proc. 20196th International Conference on Space Science and Communication*, 2019, pp. 23-28.
23. K. Sahithi, M. Sridhar, S. K.Kotamraju, K. C. S. Kavya, G. Sivavaraprasad, D. V. Ratnam, and C. Deepthi. **Characteristics of ionospheric scintillation climatology over Indian low-latitude region during the 24th solar maximum period**, *Geodesy and Geodynamics*, vol. 10, no. 2, pp. 110-117, 2019.
24. V. K. D.Srinivasu, N.Dashora, D. S. V. V.DPrasad, K. Niranjan, andS. G. Krishna. **On the occurrence and strength of multi-frequency multi-GNSS ionospheric scintillations in Indian sector during declining phase of solar cycle 24**, *Advances in Space Research*, vol. 61, no. 7,pp. 1761-1775, 2018.
25. N. Linty, A.Minetto, F.Dovis, and L.Spogli. **Effects of phase scintillation on the GNSS positioning error during the September 2017 storm at Svalbard**, *Space Weather*, vol. 16, no. 9, pp. 1317-1329, 2018.
26. R. M. Akir, M.Abdullah, K.Chellapan, A. H.Hasbi, and S. A.Bahari. **Comparative study of TEC for GISTM stations in the Peninsular Malaysia region for the period of January 2011 to December 2012**. *Advanced Science Letters*, vol. 23, no. 2,pp. 1304-1309, 2017.
27. S. Sripathi,S. Sreekumar, and S.Banola. **Characteristics of equatorial and low□latitude plasma irregularities as investigated using a meridional chain of radio experiments over India**, *Journal of Geophysical Research: Space Physics*, vol. 123, no. 5, pp. 4364-4380, 2018.
28. S. M. Buhari,M.Abdullah, Y. Otsuka, T. Yokoyama, M. Nishioka, A. M. Hasbi, and T. Tsugawa. **Detection of plasma bubble in ionosphere using GPS receivers in Southeast Asia**, *Sains Malaysiana*, vol.46, no. 6,pp. 879-88, 2017.